Society For Biomaterials

Synthesis and characterization of biomimetic citrate-based biodegradable composites

Richard T. Tran,[1]* Liang Wang,[2,3]* Chang Zhang,[4]* Minjun Huang,[2,3] Wanjin Tang,[5] Chi Zhang,[5] Zhongmin Zhang,[2,3] Dadi Jin,[2,3] Brittany Banik,[1] Justin L. Brown,[1] Zhiwei Xie,[1] Xiaochun Bai,[2,3] Jian Yang[1]

[1]Department of Bioengineering, Materials Research Institute, The Huck Institutes of The Life Sciences, The Pennsylvania State University, University Park, Pennsylvania, 16802
[2]Academy of Orthopedics, Guangdong Province, Department of Orthopedics, The Third Affiliated Hospital, Southern Medical University, Guangzhou, 510665, China
[3]Department of Cell Biology, School of Basic Medical Science, Southern Medical University, Guangzhou, 510515, China
[4]Department of Bioengineering, The University of Texas at Arlington, Arlington, Texas, 76010
[5]Texas Scottish Rite Hospital for Children, The University of Texas Southwestern Medical Center, Dallas, Texas, 75219

Received 14 July 2013; revised 7 August 2013; accepted 12 August 2013
Published online 30 August 2013 in Wiley Online Library (wileyonlinelibrary.com). DOI: 10.1002/jbm.a.34928

Abstract: Natural bone apatite crystals, which mediate the development and regulate the load-bearing function of bone, have recently been associated with strongly bound citrate molecules. However, such understanding has not been translated into bone biomaterial design and osteoblast cell culture. In this work, we have developed a new class of biodegradable, mechanically strong, and biocompatible citrate-based polymer blends (CBPBs), which offer enhanced hydroxyapatite binding to produce more biomimetic composites (CBPBHAs) for orthopedic applications. CBPBHAs consist of the newly developed osteoconductive citrate-presenting biodegradable polymers, crosslinked urethane-doped polyester and poly (octanediol citrate), which can be composited with up to 65 wt % hydroxyapatite. CBPBHA networks produced materials with a compressive strength of 116.23 ± 5.37 MPa comparable to human cortical bone (100–230 MPa), and increased C2C12 osterix gene and alkaline phosphatase gene expression *in vitro*. The promising results above prompted an investigation on the role of citrate supplementation in culture medium for osteoblast culture, which showed that exogenous citrate supplemented into media accelerated the *in vitro* phenotype progression of MG-63 osteoblasts. After 6 weeks of implantation in a rabbit lateral femoral condyle defect model, CBPBHA composites elicited minimal fibrous tissue encapsulation and were well integrated with the surrounding bone tissues. The development of citrate-presenting CBPBHA biomaterials and preliminary studies revealing the effects of free exogenous citrate on osteoblast culture shows the potential of citrate biomaterials to bridge the gap in orthopedic biomaterial design and osteoblast cell culture in that the role of citrate molecules has previously been overlooked. J Biomed Mater Res Part A: 102A: 2521–2532, 2014.

Key Words: bone tissue engineering, biodegradable composites, citric acid, osterix

How to cite this article: Tran RT, Wang L, Zhang C, Huang M, Tang W, Zhang C, Zhang Z, Jin D, Banik B, Brown JL, Xie Z, Bai X, Yang J. 2014. Synthesis and characterization of biomimetic citrate-based biodegradable composites. J Biomed Mater Res Part A 2014:102A:2521–2532.

INTRODUCTION

Introducing inorganic bioceramics, such as hydroxyapatite (HA), tricalcium phosphate (TCP), and biphasic calcium phosphates into biodegradable synthetic polymers such as poly (L-lactide) to make mechanically strong and osteoconductive materials has been a prevailing strategy in bone tissue engineering.[1–11] However, an ideal bone tissue engineered substitute that can match the native composition of bone, provide adequate mechanical support, minimize inflammatory responses, quickly promote bone regeneration, and fully integrate with the surrounding tissue is yet to be discovered.

The native bone matrix is a composite comprised of about 60–65% inorganic minerals embedded within a collagen protein matrix.[6,12–19] Previous studies have shown that

*These authors contributed equally to this work.
Correspondence to: J. Yang; e-mail: jxy30@psu.edu or X. Bai; e-mail: baixc15@smu.edu.cn
Contract grant sponsor: National Institute of Biomedical Imaging and Bioengineering (NIBIB); contract grant number: R01 award EB012575
Contract grant sponsor: National Science Foundation (NSF) CAREER award; contract grant number: 1313553
Contract grant sponsor: National Natural Sciences Foundation of China; contract grant number: 31228007
Contract grant sponsor: Arthritis Foundation
Contract grant sponsor: Texas Scottish Rite Hospital for Children; contract grant number: RAP01

a thin (3 nm thick) layer of apatite nanocrystals is embedded within the collagen network and plays important roles in controlling the mechanical properties of bone and preventing crack propagation. In the early 1960s, it was found that citrate, a well known Krebs cycle product, makes up about 5 wt % of the organic component in bone, and is responsible for regulating and stabilizing apatite nanocrystals.[20] It was later found that over 90% of the body's total citrate content is located in the skeletal system, and a more recent careful solid-state nuclear magnetic resonance study revealed that the surface of apatite nanocrystals is studded with strongly bound citrate molecules.[21–24] In addition, evidence has also shown that citrate has an innate ability to induce the HA formation in simulated body fluid (SBF).[25] Citrate is not only a dissolved calcium-solubilizing agent, but also a strongly bound and integral part of the bone nanocomposite. Surprisingly, the role of citrate is rarely mentioned in the literature related to bone cell culture and bone development in the past 30 years including those on orthopedic biomaterials and scaffolds. The natural existence of citrate and its importance in bone physiology hints that citrate should be considered in orthopedic biomaterial and scaffold design.

It is our hypothesis that a citrate-presenting polymer/HA biomaterial may better replicate the native bone citrate and inorganic mineral content to produce more biomimetic materials, which can ultimately enhance bone formation for orthopedic tissue engineering. Although our recent development of poly (1,8-octanediol citrate)–hydroxyapatite (POC–HA) composites was not driven by the above hypothesis, POC–HA did demonstrate a minimal chronic inflammatory response when implanted into a rabbit lateral femoral condyle defect model, and has been studied as a material for the fabrication of biodegradable orthopedic interference screws.[26] It was believed that the pendant carboxyl chemistry of POC prompted calcium chelation to facilitate polymer/HA interaction.[25,27–29] The improved calcium chelation resulted in its ability to incorporate up to 65 wt % HA in POC–HA composites, which is not possible with previous biodegradable lactide-based polymers ($<$ 25 wt % HA). Our recent rheological study further confirmed the presence of the calcium chelating interactions of —COOH in a citrate-based polymer, poly (ethylene glycol) maleate citrate with HA particles.[29] The favorable polymer/HA interactions induced rapid mineralization *in vitro* and promoted osteoconductivity *in vivo*. Although previous citrate materials displayed excellent biocompatibility, osteoconductivity, and osteointegration *in vivo* to provide support for our hypothesis, none of the investigated formulations could provide sufficient mechanical strength to match that of human cortical bone.[6,9,15,30–33]

Herein, we aim to develop the next generation of mechanically strong and osteoconductive citrate-presenting biomaterials based upon our recently developed crosslinked urethane-doped polyesters (CUPEs), poly (octanediol citrates) (POC), and HA.[34,35] CUPEs are a recently reported, new generation of high mechanical strength citrate-presenting biodegradable elastomers, which utilize a small amount of urethane doping to create a material 30 times stronger than the previously developed POC elastomers. Although the design and introduction of polymer/HA composites is not new, carefully selecting the candidate polymers to composite with HA at the molecular level may constitute a significant innovation in bone biomaterial design. Our results show that CBPBHA composites can address the challenges in the design of a biocompatible and mechanically strong citrate-presenting biomaterials to maximize HA incorporation and promote osteoconduction and osteointegration. It is also the first time to investigate the unexplored effects of exogenous citrate on osteoblast culture.

MATERIALS AND METHODS

Hydroxyapatite [Mw: 502.32, assay $>$ 90% (as $Ca_3(PO4)_2$); particle size: $>$ 75 μm (0.5%), 45–75 μm (1.4%), $<$ 45 μm (98.1%)] was purchased from Fluka (St. Louis, MO, USA). 1,8-octanediol (98%), citric acid (99.5%), 1,6-hexamethyl diisocyanate (HDI), and all remaining chemicals were purchased from Sigma-Aldrich (St. Louis, MO, USA) and used as received unless stated otherwise.

POC and CUPE synthesis

POC prepolymers were synthesized according to previously published methods.[35,36] Briefly, equimolar amounts of 1,8-octanediol and citric acid were added to a three-necked 100 mL round bottomed flask fitted with an inlet and outlet adapter and exposed to a constant flow of nitrogen gas. The mixture was melted under vigorous stirring at 160–165°C for 15 min. Once the constituents melted, the mixture was allowed to react at 140°C at 300 rpm for 1 h to create an unpurified low molecular weight POC prepolymer. Next, the prepolymer was added dropwise in deionized water, collected, and lyophilized overnight to obtain the purified POC prepolymer. To synthesize CUPE, POC prepolymer was first synthesized by reacting citric acid and 1,8-octanediol in a 1.0:1.1 molar ratio, respectively, and processed as stated above. Next, chain extension of the POC prepolymer was accomplished by dissolving the purified POC prepolymer in 1,4-dioxane to form a 3 wt % solution and reacting with HDI in a 1.0:1.5 POC to HDI molar ratio under constant stirring at 55°C. A Nicolet 6700 Fourier transform infrared (FTIR) spectrometer (Thermo Fisher Scientific, Waltham, MA, USA) was used to determine reaction completion when analysis of the spectra showed a disappearance of the isocyanate peak located at 2267 cm^{-1}.

CBPBHA composite fabrication

CBPBHA composites were fabricated in three distinct steps. First, a mixture of CUPE and POC prepolymers was first prepared by dissolving POC prepolymer in 1,4-dioxane and mixing with various weight ratios of CUPE prepolymer to form a homogenous citrate based polymer blend (CBPB-X, where X denotes the weight ratio of CUPE in CBPB) (Table I). In the second step, the various CBPBs were mixed with 65 wt % HA, and stirred in teflon dishes, which were prewarmed to 50°C to aid in solvent evaporation, until a

TABLE I. CBPB and CBPBHA Composite Compositions

Composite Name	CUPE (wt %)	POC (wt %)	HA (wt %)
CBPB-100	100	0	0
CBPB-90	90	10	0
CBPB-50	50	50	0
CBPB-0	0	100	0
CBPBHA-100	100	0	65
CBPBHA-90	90	10	65
CBPBHA-80	80	20	65
CBPBHA-70	70	30	65
CBPBHA-60	60	40	65
CBPBHA-50	50	50	65
CBPBHA-0	0	100	65

homogenous mixture was formed. Following solvent evaporation, the clay-like mixture was inserted into machined cylindrical metal molds and compressed into rod shaped samples. In the final step, the resulting cylindrical composites were postpolymerized at 80°C for 5 days followed by 120°C under 2 Pa vacuum for 1 day to form a crosslinked CBPBHA-X composite (where X denotes the weight ratio of CUPE in CBPB).

CBPB and CBPBHA composite characterization

Differential scanning calorimetry (DSC) measurements were conducted on a DSC Q2000 Differential Scanning Calorimeter (TA Instruments, New Castle, DE, USA) to characterize the thermal properties and homogeneity of the CBPBs. Samples were initially scanned to 150°C under nitrogen at a heating rate of 10°C min^{-1}, followed by cooling at a rate of −40°C min^{-1}, until a temperature of −75°C was achieved. Samples were then scanned again from −75 to 150°C at a heating rate of 10°C min^{-1}. The glass transition temperature (T_g) was determined from the middle of the recorded step change in heat capacity from the second heating run. To determine the miscibility of the two polymers, the blend glass transition temperature was expressed by the widely used empirical Fox equation: $1/T_g = W_1/T_{g1} + W_2/T_{g2}$ where W_i is the weight fraction of component i and the unit of temperature is Kelvin.

CBPBHA mechanical testing

Unconfined compression tests were performed using an Electromechanical Universal testing machine Q Test-150 (MTS, Eden Prairie, MN, USA). Briefly, cylindrical shaped specimens 6 × 9 mm^2 (diameter × height) were compressed at a rate of 2 mm min^{-1} to failure. The initial modulus was calculated by measuring the gradient at 10% of compression of the stress–strain curve.

CBPBHA *in vitro* degradation

The degradation rate of the 6 × 2 mm^2 (diameter × thickness) composite disk samples was assessed *in vitro* in phosphate-buffered saline (PBS) (pH 7.4) at 37°C for up to 24 weeks under static conditions. PBS was changed every week to ensure that the pH did not drop below 7. Before weighing, samples were extensively rinsed with deionized water and lyophilized. Weight loss was calculated by comparing the initial weight (W_0) with the weight measured at 1, 2, 4, 8, 12, and 24 weeks (W_t), as shown in Eq. (1). The results are presented as mean ± standard deviation ($n = 6$).

$$\text{Mass loss} = (W_0 - W_t)/W_0 \times 100\% \quad (1)$$

CBPBHA *in vitro* mineralization

In vitro mineralization of CBPBHA composites was assessed using 4× modified simulated body fluid (SBF) solution consisting of (mmol): Na+ (142.0), K+ (5.0), Mg^{2+} (1.5), Ca^{2+} (2.5), Cl^- (103), HCO^{3-} (10.0), HPO_4^{2-} (1.0) and SO_4^{2-} (0.5) with the pH adjusted to 7.0 using 1.0*M* NaOH for accelerated results.[37] Briefly, 6 × 2 mm^2 (diameter × thickness) composite disks were immersed in 10 mL of the SBF at 37°C for upto 15 days. SBF was refreshed every other day to maintain the ionic concentration and pH during mineralization. After incubation for various periods of times, the specimens were washed carefully with deionized water to remove any soluble inorganic ions and air-dried. Samples were then coated with silver and observed under a Hitachi S300N scanning electron microscope (Hitachi, Pleasanton, CA, USA). The stoichiometric Ca/P molar ratio was analyzed by energy-dispersive X-ray (EDX) analysis.

C2C12 culture on CBPBHA composites

Biomaterial films for cell culture studies were first prepared by casting prepolymer solutions in 1,4-dioxane onto circular glass cover slips, which were allowed to evaporate in a laminar flow hood. After solvent evaporation, the polymer-coated glass cover slips were crosslinked at 80°C for 2 days. The crosslinked materials were then sterilized with 70% ethanol and placed into 24-well plates. C2C12 cells (ATCC, Manassas, VA, USA) were cultured on CBPB-100, CBPBHA-100, CBPBHA-90, and control glass cover slips in high glucose Dulbecco's modified Eagle's medium (GIBCO, Grand Island, NY, USA) supplemented with 10% fetal bovine serum and 100 U/mL penicillin plus 100 μg/mL streptomycin at 95% air and 5% CO_2. The total RNA from C2C12 cells was purified using a RNeasy Mini Kit (QIAGEN, Valencia, CA, USA). RNA was subjected to quantitative real-time RT-PCR using a TaqMan One-Step RT-PCR Master Mix reagent (Applied Biosystem, Foster City, CA, USA). Relative transcript levels were analyzed by an ABI 7500 real-time PCR system (Applied Biosystem, Foster City, CA, USA). Transcript levels were normalized to glyceraldehyde-3-phosphate dehydrogenase levels. All experiments were done in duplicates and repeated three times. Osteoblast differentiation from C2C12 cells was induced by BMP-2 (R&D, Minneapolis, MN, USA) treatment.[38] After reaching 60–80% confluency, cells were treated with 300 ng mL^{-1} of BMP-2 for 0, 6, 12, 36, and 48 h. Osterix (OSX) and alkaline phosphatase (ALP) gene expression levels were analyzed as previously described.[39] The morphology of C2C12 cells on samples was visualized under scanning electron microscope (Hitachi, Pleasanton, CA, USA).

CBPB and CBPBHA citrate release

To quantify the amount of citrate release from CBPB and CBPBHA, polymer films were first prepared similar to those

prepared for the C2C12 cell culture studies. Next, the polymer films were placed into 24-well plates, and incubated in 1 mL of PBS at 37°C for 3, 7, and 14 days. At the corresponding time points, the PBS from each individual well was collected. Next, the polymer coated cover slips were thoroughly rinsed with deionized water, frozen, and lyophilized overnight. Determination of cumulative citrate released into PBS was carried out using a HP 1100 Series (Agilent, Germany) liquid chromatograph equipped with degasser, quaternary pump, autosampler adjusted to 20 μL volume injection, RP-C_{18} column (5 μm particle size, 150 × 4.6 mm^2 I.D.), and a UV-Visible diode array detector. The mobile phase consisted of a 50 m*M* PBS (pH = 2.8 adjusted with phosphoric acid), using an isocratic elution procedure with a flow rate of 0.5 mL min^{-1}. Detection of citric acid was set at 210 nm.

MG-63 culture in citrate-supplemented medium

MG-63 cells (ATCC, Manassas, VA, USA) were cultured in Eagle's Minimum Essential Media (Life Technologies, Carlsbad, CA, USA) supplemented with 10% fetal bovine serum and 100 U/mL penicillin plus 100 μg/mL streptomycin, 10 μg/mL ascorbic acid, 3 m*M* beta-glycerophosphate, and different concentrations of citric acid supplemented into media (0, 20, 100, 200, 1000, and 2000 μ*M*). At 3, 7, and 10 days, the cells were lysed and assayed for the presence of ALP using the alkaline phosphatase substrate kit (Bio-Rad, Hercules, CA, USA). The ALP levels were normalized to the total amount of DNA present in the samples as determined by a picogreen assay (Life Technologies, Carlsbad, CA, USA).

In vivo implantation

Twelve New Zealand white rabbits weighing between 2.3 and 2.7 kg were used to assess biocompatibility of CBPBHA-100 and CBPBHA-90 composites. All animal experiments were carried out in compliance with a protocol approved by Southern Medical University's Animal Care and Use Committee (Guangzhou, China). The animals were randomly divided into two groups, and anesthetized by ketamine (40 mg/kg IM) and xylazine (5–7 mg/kg IM) supplemented with isoflurane (1–2% inhalation). Next, a 1.5-cm medial incision on the lateral knee was created to expose the lateral femoral condyle. Using a mosaicplasty harvester (Smith & Nephew, Memphis, TN, USA), a 4 × 3 mm^2 (diameter × depth) bone defect was drilled in the both right and left lateral femoral condyles for the CBPBHA-100 and CBPBHA-90 group, respectively. The implants matching the dimensions of the defect were inserted according to the grouping via press fit. After all surgical procedures, the rabbits were kept in cages and maintained with a regular laboratory diet. The knees were harvested after 6 weeks of implantation and stored in 10% neutral-buffered formalin. Gross examination was documented with a digital camera. Computer tomography analysis was conducted using a Micro-CT imaging system (ZKKS-MCT-Sharp-III scanner, Caskaisheng, CHINA). The scanning system was set to 70 kV, 30 W, and 429 μA. The volume of interest was defined as bone tissue around the implants, which included the entire trabecular compartment extending 8 mm from the longitudinal axis of the implant. The extent of implant osteointegration is generally reflected by its bone-to-implant contact (BIC) measurement. BIC was calculated as the surface border length of the newly formed bone in direct contact with the implant divided by the total implant perimeter based on micro-CT images. NIH-Image software was used for image processing and analysis (National Institute of Health, Bethesda, MD, USA).

For histological analysis, paraffin-embedded decalcified tissues were cut into 4-μm-thick sections, which were then deparaffinated, hydrated, and stained with hematoxylin and eosin (H&E). For immunohistochemical (IHC) staining, paraffin-embedded sections were deparaffinated and dehydrated through a graded series of alcohol. Endogenous peroxidase activity was blocked with 0.3% hydrogen peroxide in PBS. Then, the sections were blocked with bovine serum albumin (1:100 dilution) and incubated with the primary antibody of CD68 and CD163 (Auragene, Changsha, China, 1:50 dilution) at 4°C overnight. The sections were washed with PBS three times and incubated with secondary anti-mouse IgG for 1 h at 37°C. The colorization was developed in DAB solution and counterstained by hematoxylin. Two individual pathologists assessed the inflammatory reaction surrounding the implant from H&E stained sections and IHC staining in a blinded and randomized fashion. The source of the positive control group was harvested from the healing tissue of rat's Achilles tendon 1 week post-tenotomy, which has been featured by inflammatory response. IHC staining for CD163 and CD68 was performed to detect macrophages, which appeared brown staining in the cells with hematoxylin stained nuclei.

Statistical analysis

All experiments were done in duplicates and repeated three times. Identical samples in each experiment is $n = 6$. The statistical results were based on the three experiments. Data are expressed as the mean ± standard deviation. The statistical significance between two sets of data was calculated using a two-tail Student's *t-test*. Data were taken to be significant when a $p < 0.05$ was obtained.

RESULTS

CBPBHA composite characterization

Both CUPE and POC prepolymers can be dissolved in the same polar solvents, such as 1,4-dioxane and tetrahydrofuran, and mixed together with HA to form a homogeneous CBPBHA composite after solvent evaporation and thermal crosslinking (Scheme 1). For all CBPBHA composites fabricated in this study, a 65 wt % maximum of HA was introduced into the composites, as the formulations with over 65 wt % of HA were brittle in nature and difficult to mold. The thermal properties of the different CBPB formulations absent of HA were characterized by DSC, which showed a single glass transition temperature that increased with increasing CUPE content under the same polymerization conditions (5 days, 80°C) [Fig. 1(A)]. The degradation of CBPBHA in PBS at 37°C is primarily due to the hydrolytic degradation of POC and CUPE within the

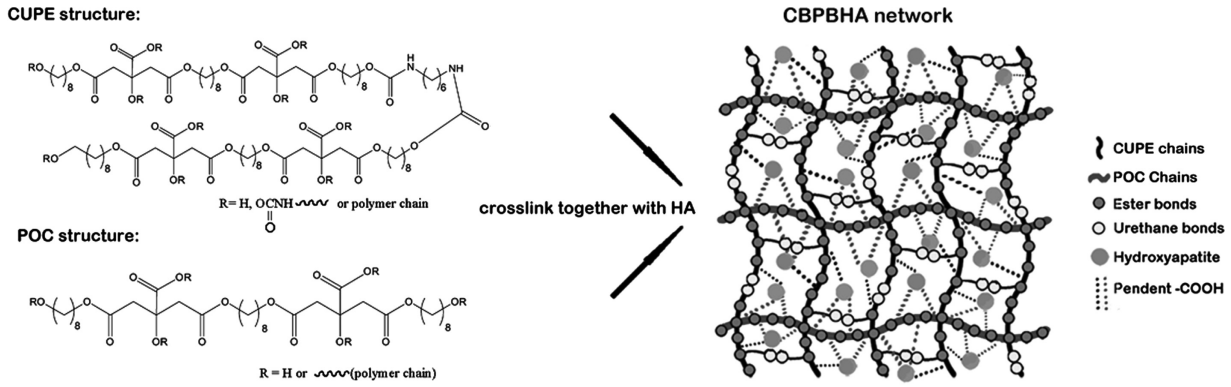

SCHEME 1. Schematic representation of CBPBHA composites.

composite. The degradation profile [Fig. 1(B)] of the CBPBHA suggested that CBPBHA slowly degraded with a total weight loss of ~6% at the end of 24 weeks. CBPBHA-90 showed more weight loss than CBPBHA-100 at initial time points, but reached weight loss equal to that of CBPBHA-100 at 24 weeks ($p > 0.05$). In all compositions of CBPBHA investigated, CBPBHA-90 displayed the highest compressive modulus and peak stress ($p < 0.05$) [Fig. 1(C,D)]. Other POC-doping ratios did not significantly alter the compressive strength of CBPBHA-(80-0) compared to CBPBHA-100 ($p > 0.05$). *In vitro* mineralization study of CBPBHA composites in SBF suggested that all the investigated formulations induced mineralization [Fig. 2(A–C)], and the Ca/P molar ratio of the mineral on CBPBHA was confirmed to be 1.39 ± 0.25 by the EDX analysis [Fig. 2(D)].

In vitro C2C12 culture on CBPB and CBPBHA films

Osteoblastic differentiation of a typical pluripotent mesenchymal cell line, C2C12, on citrate-based polymers and

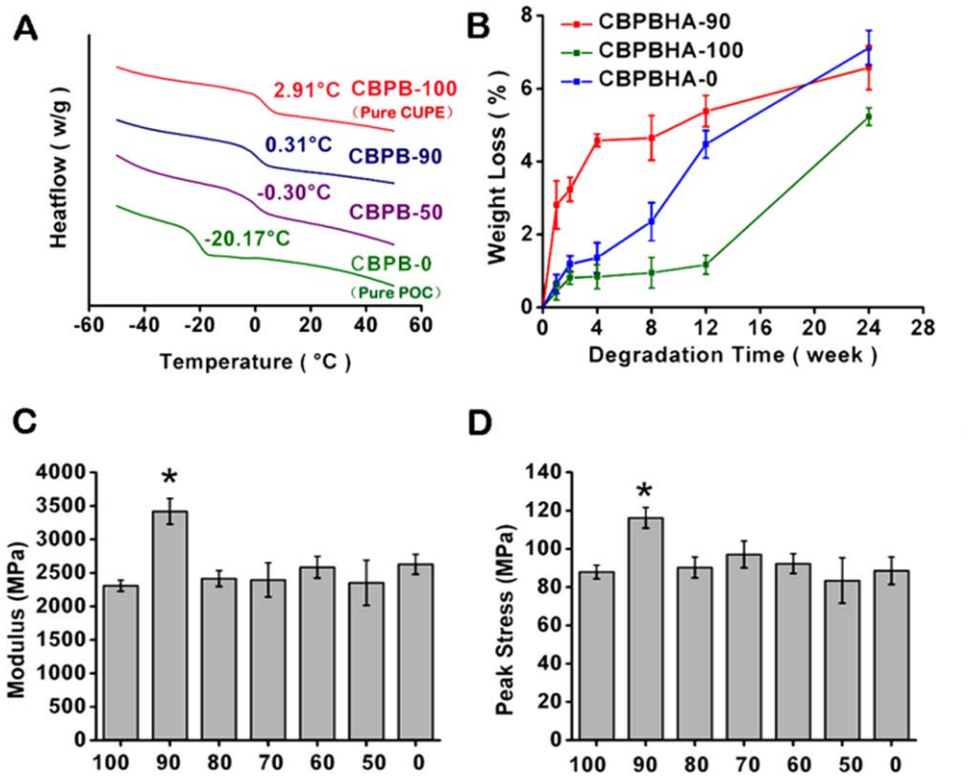

FIGURE 1. Material characterization of CBPBHA composites. A: DSC thermograms of various CBPBs. B: In vitro degradation of CBPBHA-90, CBPBHA-100, and CBPBHA-0 composites (PBS; 37°C) at 1, 2, 4, 8, 12, and 24 weeks of incubation. C: Compressive modulus of CBPBHA composites. D: Compressive peak strength of CBPBHA composites. X-axis values represent the total CUPE percentage in CBPBs. All CBPBHA composites were polymerized at 80°C for 5 days and 120°C under 2 Pa vacuum for 1 day. Data are expressed as the mean ± S.D. ($n = 6$) and (* represents significance at $p < 0.05$). [Color figure can be viewed in the online issue, which is available at wileyonlinelibrary.com.]

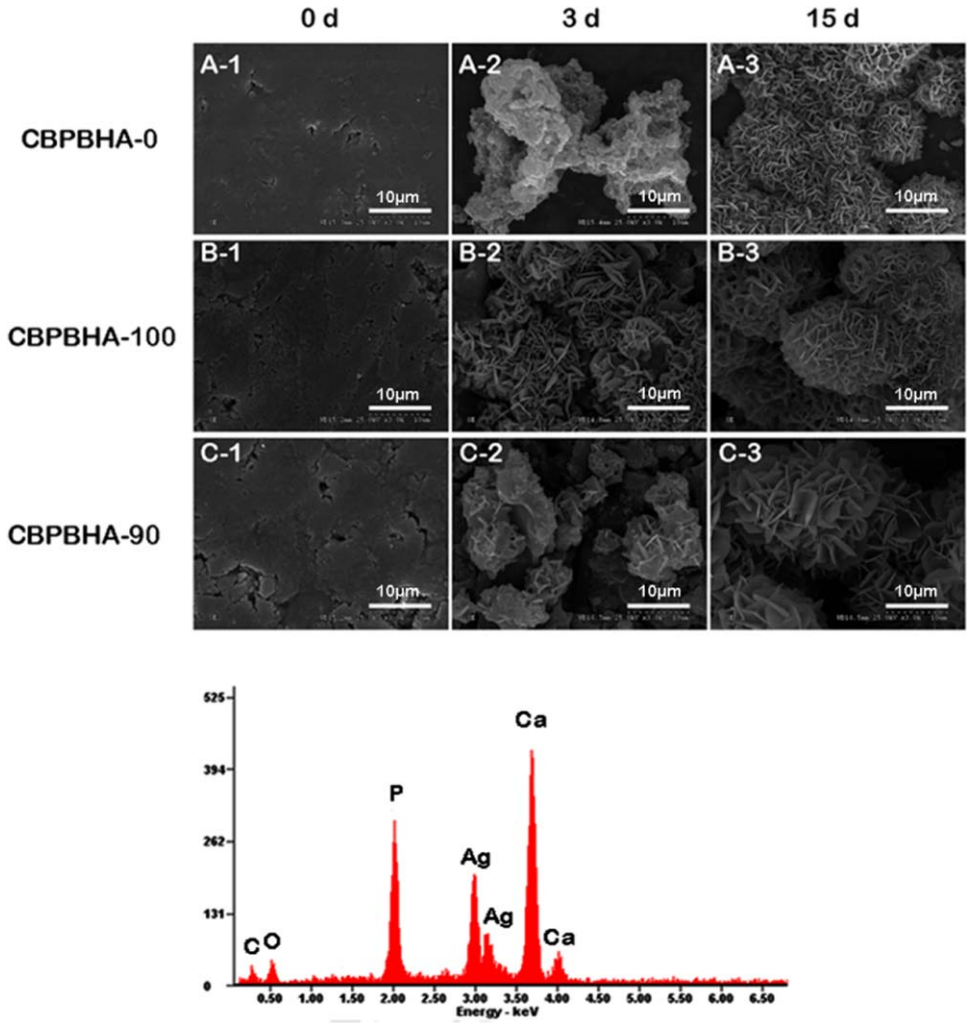

FIGURE 2. Representative SEM images of (A) CBPBHA-0, (B) CBPBHA-100, and (C) CBPBHA-90 composites mineralized in 4× simulated body fluid (SBF) at 0, 3, and 15 days. D: EDX analysis of minerals on CBPBHA-90 films incubated in SBF for 15 days. All scale bars are 10 μm. The EDX results revealed that the Ca/P ratio of apatite formed on the composites was 1.39 ± 0.25, which is comparable to octacalcium (OCP, Ca/P = 1.33) and tricalcium phosphate (TCP, Ca/P = 1.5). [Color figure can be viewed in the online issue, which is available at wileyonlinelibrary.com.]

their composites was also investigated. After 24 h, cells formed a monolayer on all CBPBHA formulations investigated [Fig. 3(A)]. ALP and OSX gene expression levels on CBPB-100 (CUPE without HA) significantly increased by 35% and 37%, respectively, compared to bare glass (control) after 48 h of culture ($p < 0.05$). With the incorporation of HA, CBPBHA-90 (CUPE/POC/HA) composite-coated plates dramatically increased ALP and OSX gene expression by 362% and 191%, respectively, whereas CBPBHA-100 (CUPE/HA) also increased gene expression levels by 336% and 290%, respectively, compared to bare glass (control) after 48 h of culture ($p < 0.01$). When compared to CBPB-100 (CUPE) coated plates after 48 h, CBPBHA-90 (CUPE/POC/HA) composites significantly increased ALP and OSX expression by 243% and 113% ($p < 0.01$), respectively, whereas CBPBHA-100 (CUPE/HA) composites increased by 224% and 185% ($p < 0.01$), respectively [Fig. 3(B,C)].

Cumulative citrate release from CBPB and CBPBHA films

To assess the amount of citrate released from the biomaterials, CBPB-90 and CBPBHA-90 films were incubated in PBS, and the cumulative citrate release was determined by HPLC over a 2-week time period. As shown in Figure 3(D), the concentration of citrate released from CBPBHA-90 was 350.87 ± 45.55 μ*M* and 477.35 ± 23.55 μ*M* by 3 and 7 days of incubation, respectively, which were both significantly higher than that of CBPB-90 ($p < 0.05$). By the 2-week time point, no significant difference in citrate release was observed between CBPB-90 and CBPBHA-90 ($p > 0.05$), which was calculated as 783.04 ± 95.31 μ*M* and 823.17 ± 107.08 μ*M* of citric acid, respectively.

Effects of exogenous citrate on osteoblastic cells

To examine the role of soluble citrate, which can be released from the biomaterial, MG-63 osteoblastic cells

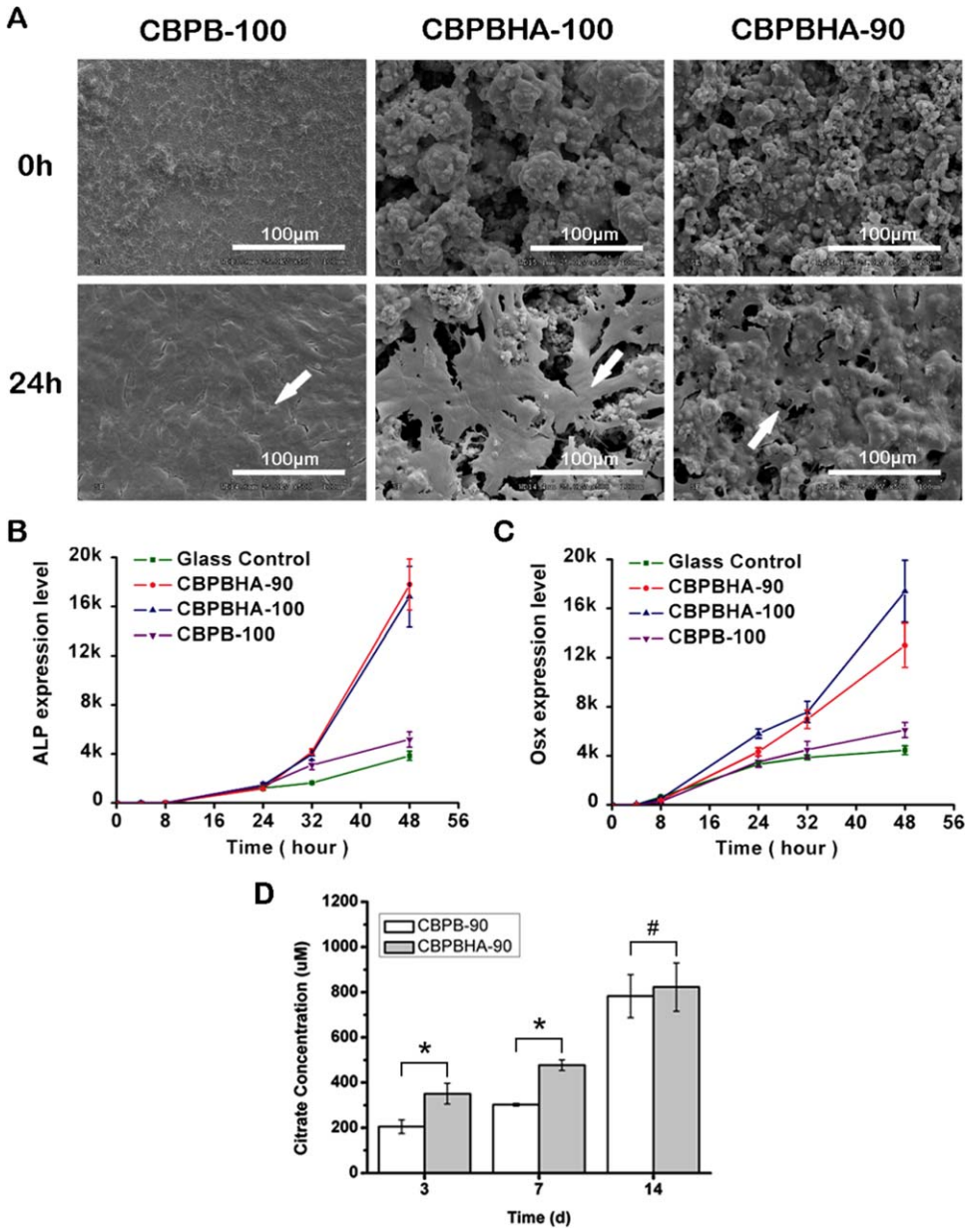

FIGURE 3. In vitro cytocompatibility and osteoblastic differentiation of C2C12s cultured on CBPB-100, CBPBHA-100, and CBPBHA-90 films. A: Representative SEM images of C2C12s 24 h post-seeding. (White arrow indicates the cell monolayer and all scale bars are 100 μm). B: Alkaline phosphatase (ALP) and (C) osterix (Osx) gene expression of C2C12s cultured on CBPB and CBPBHA films. D: Cumulative citrate release from CBPB and CBPBHA films in PBS at 37°C for 3, 7, and 14 days. Data are expressed as the mean ± S.D. ($n = 4$). * represents significance at $p < 0.05$ and # represents $p > 0.05$. [Color figure can be viewed in the online issue, which is available at wileyonlinelibrary.com.]

were cultured in citrate concentrations up to 2000 μ*M* similar to the concentrations found from citrate release studies. In the MG-63 culture, all citrate concentrations investigate displayed a significant increase in ALP production between the 3 and 7 day time points when compared to control media, which contained no citrate supplementation ($p < 0.05$). However, it was interesting to note that the 200 μ*M* displayed the highest ALP production, and was the only concentration studied to produce a significant decrease in ALP production between the 7 and 10 day time points ($p < 0.05$) (Fig. 4).

In vivo osteointegration and host response of CBPBHA composites

To assess the host response and osteointegration of the CPBPHA composites, CBPBHA-100 and CBPBHA-90 cylindrical samples were implanted into the lateral femoral condyles of rabbit knees. After 6 weeks of implantation, micro-CT images clearly showed a complete fusion of implants with surrounding new bone tissues (Fig. 5). There was no evidence of chronic inflammation (fibro-capsule formation) or degenerative changes around the implant. On gross histological examination, the implants appeared well integrated

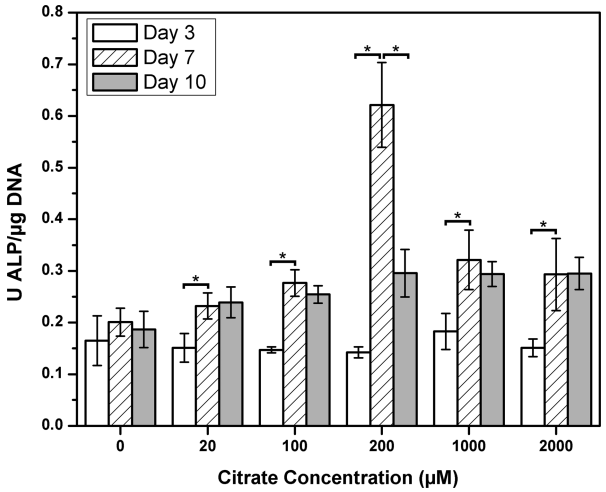

FIGURE 4. In vitro MG-63 alkaline phosphatase (ALP) production in citrate-supplemented medium over a 10 day time period (* represents significance at $p < 0.05$).

with the surrounding bone with no implant loosening detected as shown in toluidine staining and von Kossa staining for surrounding bone tissues. Bone-to-implant contact (BIC) results indicated that the bone-to-implant (osteointegration) was as high as 94.74% (Fig. 6). There was no bone resorption observed at the interface for the undecalcified bone. Excitingly, there were no positively stained macrophages (brown) found at the interface of implants and surrounding tissues (Fig. 7).

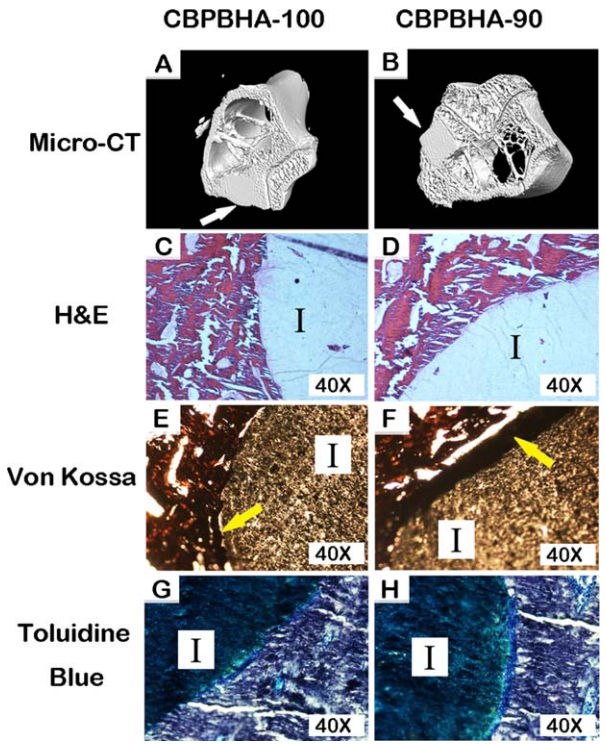

FIGURE 5. Representative 3D micro-CT and histological images demonstrating the osteointegration and foreign body response, respectively, of CBPBHA-90 and CBPBHA-100 discs implanted into a rabbit lateral femoral condyle after 6 weeks. A,B: 3D reconstructed micro-CT images, (C-D) H&E stained sections, (E,F) von Kossa stained sections, and (G,H) toluidine blue stained sections (white arrow: implants; I: Implant; yellow arrow: mineralization at the interface). [Color figure can be viewed in the online issue, which is available at wileyonlinelibrary.com.]

DISCUSSION

The incorporation of bioceramics into biodegradable polymers has been widely used to improve a material's mechanical properties and bioactivity for orthopedic applications.[40] Although promising, the current composite materials using the previous biodegradable polymers suffer from unsatisfactory mechanical strength, inefficient bone regeneration, and poor bone integration. As prior research has shown, citric acid plays an important role in inducing HA formation and regulating the thickness of apatite nanocrystals. We are the first to hypothesize that the use of citrate-based polymer in a polymer-bioceramic composite system may offer numerous benefits because of their ability to mimic the organic/inorganic composites in natural bone. Our previously developed POC–HA composites gave initial support for this hypothesis.[26] However, improving the mechanical strength of the previous POC–HA to better meet the needs of load-bearing orthopedic applications was a challenge. In fact, very few previous polymer-HA composites have shown compressive strengths in the range of native human cortical bone (100–230 MPa).[6,9,15,30–33]

Herein, we developed a new generation of citrate-based polymer blend HA composite (CBPBHA) based on CUPE, POC, and HA (Scheme 1). The rationale behind the CBPBHA bone biomaterial design are: (1) the use of citrate-presenting polymers in polymer/HA composites may mimic the organic cell niche found in natural bone to improve biocompatibility and enhance bone formation; (2) basing the composite polymer blends upon the mechanically strong urethane-doped (CUPE) polymer may increase the strength of the resulting composite to meet the needs of load-bearing orthopedic applications; (3) introducing an optimal percentage of carboxyl-rich POC into the CUPE network should significantly enhance polymer/HA interactions to better mimic the inorganic composition of bone through citrate calcium chelation, which allows for a higher percentage of HA to be incorporated in the composites when compared to previous lactide-based materials; and (4) by incorporating upto 65% HA in the composites and simulating the composition of native bone, the resulting composite may enhance osteoconduction and osteointegration.

Both CUPE and POC are citrate-based crosslinked polyester elastomers where CUPE is a urethane-doped version of POC. Although the urethane (urea)-doping chemistry sacrifices available —OH and —COOH groups in the final polymers due to the reactions between doped di-isocyanates with —OH and —COOH, CUPE is almost 30 times stronger than POC.[35,41] We initially expected to make stronger bone composite materials using CUPE with HA compared to POC–HA; however, the reduced available free —COOH and —OH in CUPE may affect the polymer's ability to chelate with

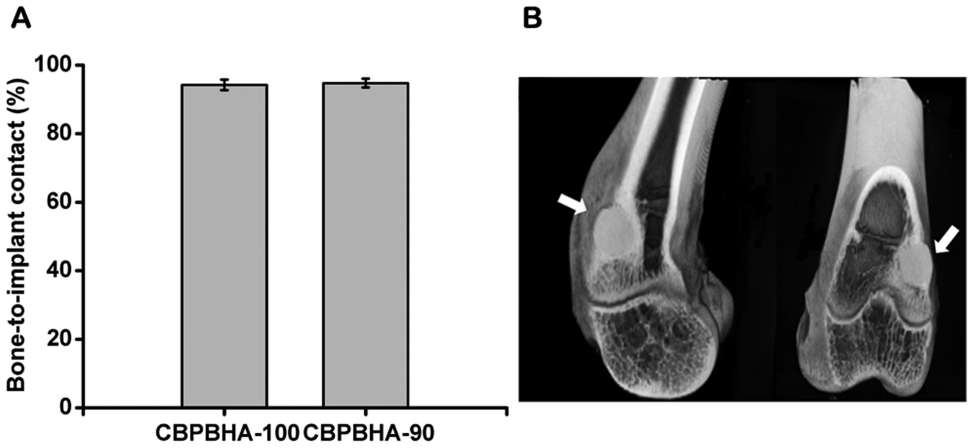

FIGURE 6. Osteointegration evaluation of CBPBHA-100 and CBPBHA-90 implants. A: Bone-to-implant contact analysis of CBPBHA-100 and CBPBHA-90 implants at 6 weeks of postimplantation. B: 2-D micro-CT images of the CBPBHA-90 implants with the surrounding bone of the lateral femoral condyle at 6 weeks of postimplantation (white arrow indicates polymer implant).

calcium-containing HA particles thus influencing the material mechanical properties.[29] Therefore, our strategy for improving the mechanical strength of POC–HA was to fabricate polymer blend HA composites by blending the —COOH rich POC with the mechanically strong CUPE to composite with HA in hopes of simultaneously achieving an optimal polymer/HA interactions and enhanced mechanical properties. CUPE and POC prepolymers can be polymerized into a homogeneous elastomeric network with no stratification or precipitation found in polymer blend process, which was further supported by a single T_g found in the DSC curves of CBPBs [Fig. 1(A)]. In the case of miscible polymer blends, the glass transition temperature of the blend can be expressed by the widely used empirical Fox equation. From this equation, the calculated T_g value for blended formulations of CBPB-90 and CBPB-50, based on the T_g of the individual components (CBPB-100 and CBPB-0), was calculated to be 0.41°C and −9.13°C, and fits this predicted T_g shift tendency. CBPBs with more CUPE showed a higher T_g as the T_g of CUPE components is higher than that of POC components in CBPBs.[35,36,42]

The compressive strength of CBPBHA-90 was 116.23 ± 5.37 MPa, which falls in the range of human cortical bone (100–230 MPa) and is a significant improvement over CBPBHA-0 (pure POC–HA composites; 88.63 ± 7.17 MPa) [Fig. 1(D)]. These results suggest that using the mechanical strong CUPE as the majority fraction greatly enhanced the mechanical strength of the composites through urethane bond incorporation. However, urethanes doping also sacrifices free carboxylic groups to chelate with HA. Because POC has more available —COOH, it acts as a binder to chelate with HA particles. Thus, CBPBHA-90 can provide better interaction with HA particles resulting in higher mechanical strength over CBPBHA-100. In the formulations studied, 10% POC in CBPBHA is sufficient to achieve the highest compressive strength.

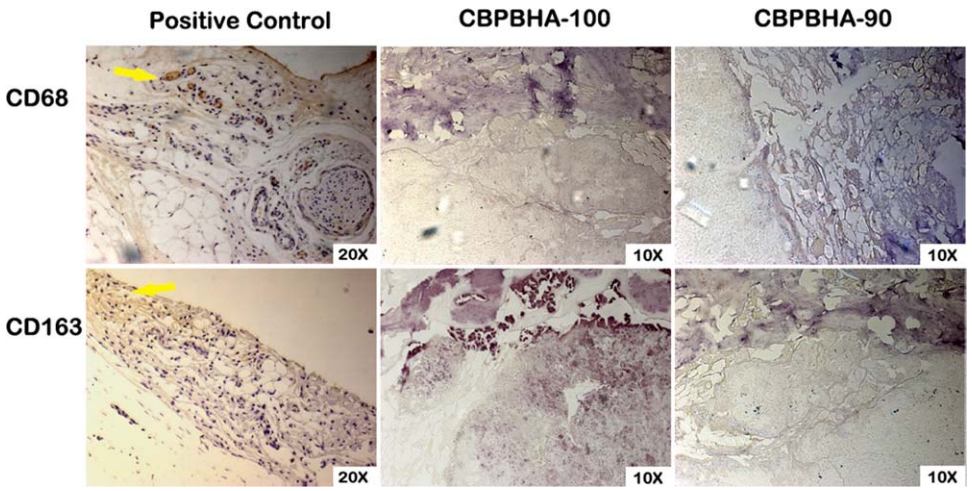

FIGURE 7. Representative images of CD68 and CD163 stained sections demonstrating the foreign body response of CBPBHA-100 and CBPBHA-90 discs implanted into a rabbit lateral femoral condyle defect after 6 weeks. Rat achilles tendon sections were used as a positive control (yellow arrow: brown-stained macrophages). [Color figure can be viewed in the online issue, which is available at wileyonlinelibrary.com.]

We have already shown that citrate-based biodegradable polymers can be degraded into monomeric forms (citrates) through a careful MALDI-MS characterization.[43] As shown in Figure 1(B), CBPBHA-100 is expected degrade slower than CBPBHA-0 as CUPE degrades slower than POC from our previous study.[35] Doping 10% POC into CBPBHA-100 resulted in a polymer blend composite (CBPBHA-90), which showed a relatively faster initial degradation rate over CBPBHA-0 (POC–HA), but significantly faster rate than CBPBHA-100. The degradation of CPBPHA composites is multifaceted and affected by the polymer types, polymer ratios, polymerization conditions, and crosslinking/chelating of polymers with HA particles. POC possesses rich —COOH that can strongly chelate/crosslink with HA particles. In CBPBHA-90, both CUPE and POC are crosslinked together by sacrificing the pendant —COOH thus reducing the chelating/crosslinking of polymers with HA particles. Therefore, CBPBHA-90 should have much less —COOH to chelate with HA and showed a faster initial degradation over CBPBHA-0. Nonetheless, all formulations studied showed slow degradation rates but can be further tuned by balancing the abovementioned parameters.[26,35,36,41]

Like many other polymer/HA composites, CBPBHA composites exhibited potential favorable osteoconductivity supported by rapid mineralization in SBF (Fig. 2).[44–46] Bone formation is a highly regulated process involving the differentiation of mesenchymal stem cells to osteoblasts.[47] ALP is an early osteoblast differentiation gene marker during bone formation, and OSX is an osteoblast-specific transcription factor required for osteoblast differentiation and bone formation.[39,48–50] In the C2C12 culture, the inclusion of HA into citrate-based polymers significantly elevated the gene expression levels and showed the potential to steer a pluripotent cell into an osteoblastic lineage [Fig. 3(B,C)] similar to many previously reported studies. However, it is worthy to note that CBPBs, without the incorporation of HA, interestingly showed increased OSX and ALP gene expression compared to glass control. It is believed that the increased bioactivity of citrate-presenting materials stems from a combination of citrate present on the biomaterial surface and the free citrate released over the course of the material degradation. To evaluate the amount of citrate typically released from the materials used in our cell culture studies, CBPB-90 and CBPBHA-90 films were chosen as candidate materials and incubated in liquid volumes mimicking those used in the C2C12 studies [Fig. 3(D)]. As determined by HPLC, CBPBHA films released higher amounts of citrate in earlier time points, which may be ascribed to the increased hydrophilicity of the material with HA incorporation.

To further explore the effects of free citrate supplemented into media on a mature osteoblast cell line, exogenous citric acid was supplemented into MG-63 medium at various concentrations to determine the effects on subsequent osteoblast ALP production. As shown in Figure 4, soluble citrate has the ability to accelerate the temporal production of ALP in MG-63s. Within the tested concentrations, 200 μM of soluble citrate supplemented into MG-63 media yielded the most ALP production and showed a significant decrease in ALP production at later time points. Although the cell culture studies performed herein are preliminary in nature, these intriguing results warrant further investigation and motivates us to further explore a mechanistic view of how citrate-based biomaterial might influence the cellular milieu for bone regeneration. Given the significant amount of citrate found in natural bone, we hypothesize that the citrate contained in and released from biodegradable citrate-based polymers may play a synergistic role with other osteogenic factors to influence bone formation.

The above exciting *in vitro* results were further supported by a 6-week *in vivo* study using a rabbit osteochondral defect model. The three-dimensional (3D) reconstructed micro-CT images [Fig. 5(A,B)] showed the formation of new bone around the composites, and bone remodeling at the calcified bone interface. Additional newly formed bone was also observed to be in contact with the implant in the bone marrow cavity, where originally there was no bone. Both CBPBHA-90 and CBPBHA-100 showed good osteointegration with the surrounding new bone. Combined with the previous mechanical test data, these results demonstrated that blending CUPE with POC to form a HA composites can greatly enhance the compressive strength of the biomaterial without altering the osteo-compatibility of the composites. As seen from Figure 5(C,D), CBPBHA implants did not induce a chronic inflammatory response (no fibrous capsule formation). From HE staining, multinucleated giant cell infiltration of both CBPBHA-90 and CBPBHA-100 implants was not evident. Fibrous capsule development was also not detected around both implants, and very minimal inflammation was generated after the implantation. New bone formation was further confirmed by toluidine blue staining [Fig. 5(E,F)] and Von Kossa staining [Fig. 5(G,H)]. Bone-to-implant analysis confirmed a large extent of interfacial bonding between bone and implants. The large view of micro-CT images also confirmed that there was no fibrous tissue between the implant and the bone or evidence of degenerative changes around the implant (Fig. 6). To further confirm the marginal inflammation produced by the two materials, CD68 and CD163, specific biomarkers for macrophage, IHC staining showed very minimal positive stained macrophages at the surrounding tissues of the implants (Fig. 7).

The above exciting *in vitro* and *in vivo* results suggest that exogenous citrate, whether presented on a biomaterial or supplemented into media, might play an unknown role in enhanced osteoblast phenotype progression, biocompatibility, osteoconduction, and osteointegration. These results are promising and may have multifaceted impacts by delineating new connections to already known factors for studying bone development. There are still no clear answers for many of the following questions: For example, what form of citrate (soluble, chemically bound, or both) influence cell differentiation and matrix production (ALP and other proteins such as osteopontin and osteocalcin)? If both have an effect, do they influence cells under the same signaling pathway or different? Do citrates exert the influences alone

or is it a synergistic response with other biochemical and biophysical cues such as growth factors, extracellular matrix components (for example bone inorganic minerals), mechanical factors, morphological structures, etc.? How will these understandings be translated into optimal biomaterial/scaffold design and bone tissue regeneration? We believe that this may be an unexplored niche in orthopedic biomaterial design. The present study focused on characterizing the new mechanically strong citrate-presenting CBPBHA composites for orthopedic applications, but also warrants future mechanism studies for bone stem cell culture and the development of an ideal orthopedic biomaterial design.

CONCLUSIONS

In this article, we describe the development of a biodegradable citrate-based polymer blend HA (CBPBHA) composites based on our newly developed crosslinked urethane-doped polyesters (CUPE), poly (octanediol citrate) (POC), and HA. The advantages of the CBPBHA composites include: (1) CBPBHA composites are based on innately biocompatible citrate-based polymers, CUPE and POC; (2) CBPBHA composites possess compressive mechanical strength in the range of reported values to that of natural cortical bone and is a major improvement over previous citrate-based materials; (3) CBPBHA composites demonstrate excellent bone integration due to their bone-mimicking compositions; (4) CBPBHA composites have the ability to incorporate a higher percent of HA (65 wt.-%) compared to the other biodegradable synthetic polymers/HA composites such as PLLA/HA (25 wt.-% HA); and (5) The addition of exogenous soluble citrate into media promotes osteoblast phenotype progression. The discovery of CBPBHA composites bridges the gap in previous bone biomaterial designs in that the role of citrate molecules was inadvertently overlooked. Future studies will focus on further understanding the role of citrate in culture medium for bone stem cell differentiation and optimizing the citrate-content in polymer/HA composites for orthopedic applications. CBPBHA composites represent a new generation of bone biomaterials that address the critical issues such as inflammation, osteoconductivity, and osteointegration. The preliminary understanding on the role of citrates in culture medium and biomaterials is instrumental and opens new avenues for future bone stem cell culture and bone biomaterial designs.

REFERENCES

1. Munch E, Launey ME, Alsem DH, Saiz E, Tomsia AP, Ritchie RO. Tough, bio-inspired hybrid materials. Science 2008;322:1516–1520.
2. Place ES, Evans ND, Stevens MM. Complexity in biomaterials for tissue engineering. Nat Mater 2009;8:457–470.
3. Tsigkou O, Pomerantseva I, Spencer JA, Redondo PA, Hart AR, O'Doherty E, Lin Y, Friedrich CC, Daheron L, Lin CP, et al. Engineered vascularized bone grafts. Proc Natl Acad Sci USA 2010; 107:3311–3316.
4. Bowles RD, Gebhard HH, Hartl R, Bonassar LJ. Tissue-engineered intervertebral discs produce new matrix, maintain disc height, and restore biomechanical function to the rodent spine. Proc Natl Acad Sci USA 2011;108:13106–13111.
5. Grayson WL, Frohlich M, Yeager K, Bhumiratana S, Chan ME, Cannizzaro C, Wan LQ, Liu XS, Guo XE, Vunjak-Novakovic G. Engineering anatomically shaped human bone grafts. Proc Natl Acad Sci USA 2009;107:3299–3304.
6. Liu H, Webster TJ. Mechanical properties of dispersed ceramic nanoparticles in polymer composites for orthopedic applications. Int J Nanomed 2010;5:299–313.
7. Rizzi SC, Heath DJ, Coombes AG, Bock N, Textor M, Downes S. Biodegradable polymer/hydroxyapatite composites: Surface analysis and initial attachment of human osteoblasts. J Biomed Mater Res 2001;55:475–486.
8. Saito M, Maruoka A, Mori T, Sugano N, Hino K. Experimental studies on a new bioactive bone cement: Hydroxyapatite composite resin. Biomaterials 1994;15:156–160.
9. Wagoner Johnson AJ, Herschler BA. A review of the mechanical behavior of CaP and CaP/polymer composites for applications in bone replacement and repair. Acta Biomater 2011;7:16–30.
10. Saito N, Okada T, Horiuchi H, Murakami N, Takahashi J, Nawata M, Ota H, Nozaki K, Takaoka K. A biodegradable polymer as a cytokine delivery system for inducing bone formation. Nat Biotechnol 2001;19:332–335.
11. Gentleman E, Swain RJ, Evans ND, Boonrungsiman S, Jell G, Ball MD, Shean TA, Oyen ML, Porter A, Stevens MM. Comparative materials differences revealed in engineered bone as a function of cell-specific differentiation. Nat Mater 2009;8:763–770.
12. Bhumiratana S, Grayson WL, Castaneda A, Rockwood DN, Gil ES, Kaplan DL, Vunjak-Novakovic G. Nucleation and growth of mineralized bone matrix on silk-hydroxyapatite composite scaffolds. Biomaterials 2011;32:2812–2820.
13. Brauer DS, Russel C, Vogt S, Weisser J, Schnabelrauch M. Fabrication and in vitro characterization of porous biodegradable composites based on phosphate glasses and oligolactide-containing polymer networks. J Biomed Mater Res A 2007;80:410–420.
14. Chesnutt BM, Viano AM, Yuan Y, Yang Y, Guda T, Appleford MR, Ong JL, Haggard WO, Bumgardner JD. Design and characterization of a novel chitosan/nanocrystalline calcium phosphate composite scaffold for bone regeneration. J Biomed Mater Res A 2009;88:491–502.
15. Kane RJ, Converse GL, Roeder RK. Effects of the reinforcement morphology on the fatigue properties of hydroxyapatite reinforced polymers. J Mech Behav Biomed Mater 2008;1:261–268.
16. Katti KS, Katti DR, Dash R. Synthesis and characterization of a novel chitosan/montmorillonite/hydroxyapatite nanocomposite for bone tissue engineering. Biomed Mater 2008;3:034122.
17. Liang SL, Cook WD, Thouas GA, Chen QZ. The mechanical characteristics and in vitro biocompatibility of poly(glycerol sebacate)-bioglass elastomeric composites. Biomaterials 2010;31:8516–8529.
18. Witte F, Feyerabend F, Maier P, Fischer J, Stormer M, Blawert C, Dietzel W, Hort N. Biodegradable magnesium-hydroxyapatite metal matrix composites. Biomaterials 2007;28:2163–2174.
19. Rezwan K, Chen QZ, Blaker JJ, Boccaccini AR. Biodegradable and bioactive porous polymer/inorganic composite scaffolds for bone tissue engineering. Biomaterials 2006;27:3413–3431.
20. Hartles RL. Citrate in mineralized tissues. Adv Oral Biol 1964;1: 225–253.
21. Dickens F. The citric acid content of animal tissues, with reference to its occurrence in bone and tumour. Biochem J 1941;35:1011–1023.
22. Eastoe JE, Eastoe B. The organic constituents of mammalian compact bone. Biochem J 1954;57:453–459.
23. Dixon TF, Perkins HR. Citric acid and bone metabolism. Biochem J 1952;52:260–265.
24. Hu YY, Rawal A, Schmidt-Rohr K. Strongly bound citrate stabilizes the apatite nanocrystals in bone. Proc Natl Acad Sci USA 2010;107:22425–22429.
25. Rhee SH, Tanaka J. Effect of citric acid on the nucleation of hydroxyapatite in a simulated body fluid. Biomaterials 1999;20: 2155–2160.
26. Qiu H, Yang J, Kodali P, Koh J, Ameer GA. A citric acid-based hydroxyapatite composite for orthopedic implants. Biomaterials 2006;27:5845–5854.
27. Rhee SH, Tanaka J. Hydroxyapatite formation on cellulose cloth induced by citric acid. J Mater Sci Mater Med 2000;11:449–452.
28. Yokoyama A, Yamamoto S, Kawasaki T, Kohgo T, Nakasu M. Development of calcium phosphate cement using chitosan and

citric acid for bone substitute materials. Biomaterials 2002;23: 1091–1101.
29. Jiao Y, Gyawali D, Stark JM, Akcora P, Nair P, Tran RT, Yang J. A rheological study of biodegradable injectable PEGMC/HA composite scaffolds. Soft Matter 2012;8:1499–1507.
30. Nandi SK, Roy S, Mukherjee P, Kundu B, De DK, Basu D. Orthopaedic applications of bone graft & graft substitutes: A review. Indian J Med Res 2010;132:15–30.
31. Hutmacher DW, Schantz JT, Lam CX, Tan KC, Lim TC. State of the art and future directions of scaffold-based bone engineering from a biomaterials perspective. J Tissue Eng Regen Med 2007;1: 245–260.
32. Childs THC, Arola D. Machining of cortical bone: Simulations of chip formation mechanics using metal machining models. Mach Sci Technol 2011;15:206–230.
33. Zioupos P, Gresle M, Winwood K. Fatigue strength of human cortical bone: Age, physical, and material heterogeneity effects. J Biomed Mater Res A 2008;86:627–636.
34. Webb AR, Yang J, Ameer GA. Biodegradable polyester elastomers in tissue engineering. Expert Opin Biol Ther 2004;4:801–812.
35. Dey J, Xu H, Shen J, Thevenot P, Gondi SR, Nguyen KT, Sumerlin BS, Tang L, Yang J. Development of biodegradable crosslinked urethane-doped polyester elastomers. Biomaterials 2008;29:4637–4649.
36. Yang J, Webb AR, Pickerill SJ, Hageman G, Ameer GA. Synthesis and evaluation of poly(diol citrate) biodegradable elastomers. Biomaterials 2006;27:1889–1898.
37. Oyane A, Kim HM, Furuya T, Kokubo T, Miyazaki T, Nakamura T. Preparation and assessment of revised simulated body fluids. J Biomed Mater Res A 2003;65:188–195.
38. Ryoo HM, Lee MH, Kim YJ. Critical molecular switches involved in BMP-2-induced osteogenic differentiation of mesenchymal cells. Gene 2006;366:51–57.
39. Tang W, Li Y, Osimiri L, Zhang C. Osteoblast-specific transcription factor Osterix (Osx) is an upstream regulator of Satb2 during bone formation. J Biol Chem 2011;286:32995–33002.
40. Chung EJ, Sugimoto MJ, Ameer GA. The role of hydroxyapatite in citric acid-based nanocomposites: Surface characteristics, degradation, and osteogenicity in vitro. Acta Biomater 2011;7:4057–4063.
41. Dey J, Tran RT, Shen J, Tang L, Yang J. Development and long-term in vivo evaluation of a biodegradable urethane-doped polyester elastomer. Macromol Mater Eng 2011;296:1149–1157.
42. Ao ZM, Jiang Q. Size effects on miscibility and glass transition temperature of binary polymer blend films. Langmuir 2006;22: 1241–1246.
43. Serrano CA, Zhang Y, Yang J, Schug KA. Matrix-assisted laser desorption/ionization mass spectrometric analysis of aliphatic biodegradable photoluminescent polymers using new ionic liquid matrices. Rapid Commun Mass Spectrom 2011;25:1152–1158.
44. Suzuki O. Octacalcium phosphate: Osteoconductivity and crystal chemistry. Acta Biomater 2010;6:3379–3387.
45. LeGeros RZ. Properties of osteoconductive biomaterials: Calcium phosphates. Clin Orthop Relat Res 2002;395:81–98.
46. Imaizumi H, Sakurai M, Kashimoto O, Kikawa T, Suzuki O. Comparative study on osteoconductivity by synthetic octacalcium phosphate and sintered hydroxyapatite in rabbit bone marrow. Calcif Tissue Int 2006;78:45–54.
47. Zhang C. Transcriptional regulation of bone formation by the osteoblast-specific transcription factor Osx. J Orthop Surg Res 2010;5:37.
48. Nakashima K, Zhou X, Kunkel G, Zhang Z, Deng JM, Behringer RR, de Crombrugghe B. The novel zinc finger-containing transcription factor osterix is required for osteoblast differentiation and bone formation. Cell 2002;108:17–29.
49. Zhou X, Zhang Z, Feng JQ, Dusevich VM, Sinha K, Zhang H, Darnay BG, de Crombrugghe B. Multiple functions of Osterix are required for bone growth and homeostasis in postnatal mice. Proc Natl Acad Sci USA 2010;107:12919–12924.
50. Baek WY, Lee MA, Jung JW, Kim SY, Akiyama H, de Crombrugghe B, Kim JE. Positive regulation of adult bone formation by osteoblast-specific transcription factor osterix. J Bone Miner Res 2009;24:1055–1065.